

## Stacking in sediments of colloidal hard spheres

Matthieu Marechal,<sup>a)</sup> Michiel Hermes, and Marjolein Dijkstra

*Soft Condensed Matter, Debye Institute for NanoMaterials Science, Utrecht University, Princetonplein 5, 3584 CC Utrecht, The Netherlands*

(Received 29 April 2011; accepted 17 June 2011; published online 21 July 2011)

We use computer simulations to investigate the crystallization dynamics of sedimenting hard spheres in large systems (hundreds of thousands of particles). We show that slow sedimentation results primarily in face-centered cubic (fcc) stacked crystals, instead of random hexagonal close packed or hexagonal close packed (hcp) crystals. We also find slanted stacking faults, in the fcc regions. However, we attribute the formation of fcc to the free energy difference between fcc and hcp and not to the presence of these slanted stacking faults. Although the free energy difference between hcp and fcc per particle is small (only  $10^{-3}$  times the thermal energy), it can become considerable, when multiplied by the number of particles in each domain. The ratio of fcc to hcp obtained from dynamic simulations is in excellent agreement with well-equilibrated Monte Carlo simulations, in which no slanted stacking faults were found. Our results explain a range of experiments on colloids, in which the amount of fcc increases upon lowering the sedimentation rate or decreasing the initial volume fraction. © 2011 American Institute of Physics. [doi:10.1063/1.3609103]

### I. INTRODUCTION

The bulk phase behavior of hard spheres has been studied in great detail and is well-understood by now. In particular, it was shown by computer simulations that such a system shows a purely entropy-driven phase transition from a disordered fluid phase to a face-centered-cubic (fcc) crystal phase at sufficiently high densities.<sup>1–3</sup> Although the fcc phase is the most stable phase, the free energy difference with respect to the metastable hexagonal-close-packed (hcp) structure is only very small, on the order of  $10^{-3}k_B T$  per particle at the melting transition.<sup>4</sup> Here, we define  $k_B$  as Boltzmann's constant and  $T$  as the temperature. Computer simulations of hard spheres have shown that crystals formed spontaneously in a supersaturated fluid predominantly have a random-hexagonal-close-packed (rhcp) structure.<sup>5,6</sup>

Suspensions of colloidal particles can serve as excellent experimental realizations of the hard-sphere system as the effective interactions of the colloids can be tuned in such a way that the particles interact approximately as hard spheres.<sup>7,8</sup> However, gravity is often non-negligible in colloidal suspensions, as in most common solvents the gravitational energy corresponding to a height difference of about one colloid diameter is comparable to the thermal energy for micron sized colloidal particles. Hence, a spatial inhomogeneous suspension is obtained due to the gravitational field. The parameter that is associated with a gravitational field is the so-called gravitational length and reads  $\ell/\sigma = (\beta mg\sigma)^{-1}$ , where  $m$  is the effective or buoyant mass of the colloidal particles,  $\beta = (k_B T)^{-1}$ ,  $\sigma$  is the diameter of the colloids, and  $g$  is the gravitational acceleration. The Peclet number  $Pe_\sigma \equiv \sigma/\ell$  is also used. If a gravitational field is applied to a fluid of colloidal particles,<sup>9–18</sup> the density will become inhomogeneous.

Furthermore, if, due to the gravitational field, the density at the bottom increases sufficiently, the system can start to crystallize upwards from the bottom.

Crystallization in sediments of hard spheres was studied using Monte Carlo (MC) simulations and density functional theory<sup>12–16,18</sup> and for colloids by confocal microscopy.<sup>19,20</sup> The simulations in Ref. 12 show a discontinuous transition where the first two layers crystallize at the same gravitational field strength. Upon increasing the gravitational field further, the crystalline film grows continuously. However, in contrast with the simulation results<sup>12</sup> density functional theory predicts discontinuous crystal growth via layering transitions upon increasing gravity. In a recent simulation study,<sup>21</sup> the freezing transition in suspensions of hard spheres was investigated in more detail. This study supported the continuous layer-by-layer growth as found in the Monte Carlo simulations of Biben *et al.*<sup>12</sup> Furthermore, it was shown that the chemical potential  $\mu$  at which the  $n$ th layer crystallizes can be predicted by a simple expression, which we will use to grow a crystal of hard spheres in a controlled layer-by-layer fashion in this study.

Stacking faults are irregularities in the way in which crystalline layers are stacked on top of each other. In this work, we will consider fcc to be the defect-free crystal, since it is the equilibrium structure (even though the free energy difference with hcp is very small). A stacking fault in a fcc crystal is a juxtaposition of two hcp layers.<sup>22</sup> Colloids that exhibit hard sphere-like interactions are an ideal system for studying stacking faults, since the free energy for a stacking fault<sup>23</sup> is only around  $10^{-4}k_B T/a^2$ , where  $a$  is the lattice constant of a hard-sphere crystal. For comparison, face-centered-cubic atomic systems, such as Cu (Ref. 24) and  $\gamma$ -Fe,<sup>25</sup> have a stacking fault energy of several  $k_B T/a^2$ , limiting the size of mis-stacked domains to a few unit cells. The stacking of colloidal crystals as found in natural opals<sup>26</sup> as well as self-assembled<sup>20,27–33</sup> and convectively assembled<sup>34,35</sup> crystals

<sup>a)</sup> Author to whom correspondence should be addressed. Electronic mail: marechal@thphy.uni-duesseldorf.de.

of synthetic colloids has been extensively investigated experimentally.

The effect of gravity on the stacking of colloidal crystals has been made apparent by comparing crystals grown on earth to those grown in reduced gravity. Reduced gravity can be achieved either by adjusting the mass density of the solvent to be almost equal to the mass density of the colloids,<sup>27,31</sup> by performing the experiments in microgravity<sup>36–39</sup> or even by applying an electrophoretic force opposing gravity.<sup>40</sup> It should also be noted that the particle diameter  $\sigma$  ranges from 200 nm to 1  $\mu\text{m}$ , which implies that the Peclet number ( $\propto \sigma^4$ ) can change by three orders of magnitude depending on the diameter. Crystals grown in reduced gravity show random stacking with almost equal probabilities to find fcc and hcp (Refs. 27 and 36) at least in the first few days after the onset of the crystallization.<sup>37</sup> The experiments with a non-negligible gravitational field seem to fall in roughly three categories, (i) slow sedimentation starting from a low volume fraction or with a small Peclet number; (ii) fast sedimentation starting with a volume fraction below the density of the bulk fluid at coexistence with the crystal; and (iii) experiments that have an initial volume fraction that lies above the coexistence density of the fluid. In case (i), heterogeneous nucleation occurs at the bottom wall and mostly fcc grows.<sup>28–30</sup> Randomly stacked crystals grow upon fast sedimentation after nucleation at the bottom wall in case (ii) and, finally, in case (iii), homogeneous nucleation of rhcp in the bulk of the sample occurs as well as heterogeneous nucleation at the wall. It is worth noting here that a recent simulation study shows that the critical crystal nucleus which forms in the bulk of a supersaturated hard-sphere fluid is predominantly fcc-like.<sup>41</sup> However, the nucleus grows out to a mostly rhcp crystal with only a small preference for fcc. The rhcp crystal formed in cases (ii) and (iii) as well as under reduced gravity, slowly transforms to fcc (Refs. 31, 32, 37, 38, and 42) as predicted by Pronk and Frenkel.<sup>23</sup> However, the rate at which this transition occurs is usually higher than expected, which has been explained by the mechanical perturbations that are unavoidable during manual handling of the sample.<sup>32</sup>

Homogeneous nucleation during sedimentation is difficult to interpret and can only be related to the bulk behavior in a simple way using an extrapolation to the time of homogenization.<sup>43</sup> A crystallite of colloids will have a higher mass density than the surrounding colloidal fluid phase, because the number density in the crystal is larger than that in the fluid. Even though this density difference is small, the net gravitational force on the crystallite will become important during some stage of the crystallization (even if the gravitational length is large), as the net mass of the crystallite will increase with its radius cubed, while its drag coefficient scales only linearly with its radius. The resulting sedimentation velocity difference between a crystallite and the surrounding colloidal fluid phase might cause sufficient shear near the surface of the crystallite to affect the stacking.<sup>32</sup> Simulations on these types of systems would require full calculations of the hydrodynamic interactions for large numbers of particles and would be prohibitively slow. Therefore, we focus on systems with initial volume fractions below bulk coexistence, in which

the crystallization occurs at the wall and the hydrodynamic interactions play a minor role.

When the initial volume fraction is low, the structure of the crystal seems to be mainly influenced by a parameter introduced by Hoogenboom *et al.*,<sup>28</sup> the product of the initial volume fraction, and the Peclet number, which is proportional to the flux of particles from the homogeneous, sedimenting bulk fluid onto the sediment. When this flux is low, the system has time to equilibrate and the fraction of fcc is large, whereas predominantly randomly stacked layers are found if the particle flux is high. Interestingly, observation by both x-ray scattering<sup>33</sup> and confocal microscopy<sup>20</sup> indicates that these randomly stacked layers are grouped and that these regions of randomly stacked layers are intermixed with regions of almost pure fcc with a single stacking direction (i.e., no twinning defects) for intermediate sedimentation fluxes. Hilhorst *et al.*, showed that these fcc regions often contain a slanted stacking fault, that is a stacking fault (2 subsequent hcp stacked layers) which runs along one of the  $(\bar{1}11)$ ,  $(1\bar{1}1)$ , or  $(11\bar{1})$  planes, if the  $(111)$  plane is aligned with the bottom wall. As the crystal grows up from the bottom wall, it grows along the slanted stacking fault and in this way, Hilhorst *et al.*<sup>20</sup> proposed that the stacking is forced to be fcc with a fixed stacking direction (see Sec. III A and Ref. 44). Although slanted stacking faults in colloidal systems were first observed<sup>45</sup> as misfit dislocations<sup>46,47</sup> that relieve stress due to an ill-fitting template, Hilhorst *et al.* argued that slanted stacking faults can also originate from a line where two differently stacked domains meet.<sup>20</sup>

In this work, we study the crystalline structure of sediments of hard spheres as obtained from dynamic simulations. To this end, we have employed a simulation method where event driven molecular dynamics are extended with Brownian motion. Using this method, we are able to achieve system sizes large enough to investigate spontaneously grown defect structures, such as slanted stacking faults.<sup>20</sup> We confirm the increase in the fraction of fcc stacked particles  $\alpha = N_{\text{fcc}}/N_{\text{crystal}}$  with decreasing initial volume fraction as observed in experiments. Second, slanted stacking faults are found using a combination of order parameters and their number is shown to be correlated with the amount of fcc stacked layers. However, we propose an alternative explanation for the increase of the fraction of fcc with decreasing volume fraction: the amount of fcc is simply determined by the small bulk free energy difference per particle between hcp and fcc multiplied by the size of a typical domain. A slanted stacking fault is then simply a type of defect that can only occur in fcc crystallites and not in hcp regions. Three-layer stacking probabilities are shown to be in agreement with the bulk free energies from Ref. 48. As further proof of the role of the bulk free energy in determining the stacking of sedimented hard sphere crystals, we perform Monte Carlo simulations similar to the ones performed for dumbbells under gravity.<sup>49</sup> A large probability for a layer to stack fcc-like was also found in these simulations, in which no slanted stacking faults were formed. Finally, the results of Hilhorst *et al.*<sup>20</sup> are reinterpreted by assuming a distribution of domain sizes: domain sizes above the critical domain size for the formation of fcc are predominantly fcc

stacked, domains smaller than this critical size are randomly stacked.

## II. SIMULATION METHODS

### A. Model

We consider a system of hard spheres with diameter  $\sigma$  in a gravitational field oriented along the  $z$ -direction. The spheres are confined between two smooth hard parallel walls at  $z = 0$  and  $z = H$  and are subjected to the external potential:

$$\phi(z) = \begin{cases} mgz, & \sigma/2 \leq z \leq H - \sigma/2 \\ \infty, & \text{otherwise} \end{cases}, \quad (1)$$

where  $z$  is the vertical coordinate,  $g$  is the gravitational acceleration, and  $m$  is the buoyant mass of the hard spheres. The height  $H$  is chosen such that the final density at the top of the box  $\rho(z = H - \sigma/2)$  is negligibly small and thus the system can be considered to be infinite in the  $z$ -direction. The Peclet number was  $Pe_\sigma = 1$  for all simulations considered unless stated otherwise. This value of the Peclet number corresponds to the lighter of the two types of colloids of Hoogenboom *et al.*<sup>28</sup>

The event driven Brownian dynamics simulations (see below) were performed in the  $NVT$  ensemble, using a number of particles  $N = 10^5$  or  $4 \times 10^5$ , while the simulation box had a horizontal area of  $A = 50\sigma \times 50\sigma$  or  $100\sigma \times 100\sigma$ , such that the number of particles per area was always  $40/\sigma^2$ . The initial configurations of these simulations were homogeneous fluids with initial volume fractions  $\phi_i = 0.010467, 0.02, 0.05, \text{ and } 0.2$ . A volume of  $A \times (H - \sigma)$  was randomly filled with  $N = 10^5$  or  $4 \times 10^5$  non-overlapping spheres up to a certain density for a height  $H - \sigma$ . Unless specified otherwise, all event driven Brownian dynamics simulations (see Sec. III B) were performed with the lowest initial volume fraction ( $\phi_i \simeq 0.01$ ). This initial volume fraction was chosen to match the experimental conditions of Hoogenboom *et al.*<sup>28</sup> MC simulations were performed in both the  $NVT$  and  $\mu VT$  (grand canonical) ensemble. Using  $NVT$  MC simulations, the effect of gravity on perfect crystals was studied; therefore, the bottom part of the simulation box was filled with an initially perfect crystal of 60 layers with a lattice constant of  $1.06\sigma$  or  $1.1\sigma$ . The lateral dimensions of the simulation box in all types of MC simulations were chosen to match a perfect hexagonal layer with dimensions  $na \times m\sqrt{3}a$ , for integers  $n, m$ . The  $\mu VT$  MC simulations<sup>21</sup> (in which the number of particles varies to maintain a constant chemical potential  $\mu$ ) were used to grow a well-equilibrated crystal in a series of simulations by increasing the chemical potential, such that exactly a single crystalline layer grows during each simulation. The initial configuration of the first run of this series consisted of a well-equilibrated fluid-like sediment.

### B. Sedimentation versus crystallization

The faster the sedimentation and the higher the initial volume fraction, the less time the sediment has available for equilibration during the sedimentation. To quantify the available

time for equilibration, we define the dimensionless particle flux as

$$J = v_d \rho_i \sigma^2 \tau_s^L, \quad (2)$$

where  $v_d$  is the sedimentation velocity and  $\rho_i$  is the initial number density. The flux  $J$  is equal to the number of particles that traverse an area equal to the diameter squared  $\sigma^2$  in a time  $\tau_s^L = \sigma^2/(6D_s^L)$ , where  $D_s^L$  is the long time self-diffusion constant. We use the long-time self-diffusion constant  $D_s^L$  of the fluid just below coexistence with the crystal (with  $\phi \simeq 0.49$ ) in Eq. (2), since we are interested in rearrangements during crystallization. Measurements of  $D_s^L$  in experiments have been performed for this packing fraction, which resulted in  $D_s^L/D_0 \simeq 0.051$ ,<sup>50</sup> where  $D_0 = k_B T/(6\pi\eta R)$  is the Stokes-Einstein diffusion constant with the dynamic viscosity  $\eta$  and the radius of the colloids  $R = \sigma/2$ . We measured  $D_s^L$  in our event driven Brownian dynamics simulations and obtained  $D_s^L/D_0 = 0.03252(1)$  (the difference is due to the simulation method, see Sec. III B). For high values of  $J$  we expect small crystalline domains and many defects or even a glass, while for low values we expect large crystalline domains with few defects. Another motivation for using  $J$  to characterize the deviation from equilibrium can be given by noting that  $J$  is approximately equal to the time that is needed to equilibrate a layer divided by the time that is available for equilibration. We assume that local equilibrium is reached after a time  $\tau_s^L$ , which then corresponds to the required time to equilibrate a layer of particles. The time available for equilibration is of the order of the sedimentation time of a layer  $\tau_{\text{sed}} = N_{\text{lay}}/(\rho_i v_d A)$ , where  $N_{\text{lay}}$  is the number of particles in a layer with area  $A$ . Dividing  $\tau_s^L$  by  $\tau_{\text{sed}}$  and using  $A \simeq N_{\text{lay}}\sigma^2$  for hard spheres, one obtains  $J$ . The dimensionless flux  $J$  can be written in terms of the Peclet number  $Pe_\sigma = v_d \sigma/D_0$ , the initial volume fraction  $\phi_i$ , and  $D_s^L/D_0$ :

$$J = Pe_\sigma \frac{D_0}{D_s^L} \frac{\phi_i}{\pi} \simeq \frac{\tau_s^L}{\tau_{\text{sed}}}. \quad (3)$$

The values for  $J$  of this work are compared to those of three experimental studies in Table I. In all experimental studies where  $J$  is considerably smaller than one, large amounts of fcc crystals were found, while for  $J > 1$  no preference for fcc was found. For the experimental study,<sup>20</sup>  $J$  varied between 0.12 and 0.62 and indeed both fcc and rhcp crystallites were found, such that the average stacking parameter is between 0.5 and 1.

Note that the definitions of the Brownian time and the Peclet number that are used in the literature<sup>19,51,52</sup> vary by constant factors of order unity. For instance, Hoogenboom *et al.*<sup>28</sup> used  $\Delta\rho g R^4/k_B T$  for the Peclet number, such that their definition of the Peclet number differs from ours by a factor of about 8.

### C. Event driven Brownian dynamics (BD) simulations

Experiments on colloidal hard spheres have been performed to study certain types of defects in colloidal crystals.<sup>20,53–55</sup> Furthermore, these defects have been claimed to have an effect on the stacking of colloidal crystals.<sup>20</sup> A

TABLE I. The Peclet number  $Pe_\sigma$ , initial volume fraction  $\phi_i$ , and the dimensionless particle flux due to sedimentation  $J$  [Eqs. (2) and (3)] of the simulations in this work, which are compared to those of the experiments from Refs. 20, 28, and 29.

|                 | $Pe_\sigma$ | $\phi_i$           | $J$                |
|-----------------|-------------|--------------------|--------------------|
| This work       | 1.015       | 0.0105             | 0.104              |
|                 | 1.015       | 0.020              | 0.199              |
|                 | 1.015       | 0.051              | 0.503              |
|                 | 1.015       | 0.2                | 1.987              |
|                 | 0.5008      | 0.104              | 0.518              |
|                 | 0.5008      | 0.207              | 1.030              |
| Expt. (Ref. 28) | 1.1         | 0.002              | 0.014              |
|                 | 1.1         | 0.004              | 0.027              |
|                 | 4.19        | 0.005              | 0.13               |
|                 | 4.19        | 0.026              | 0.68               |
|                 | 4.19        | 0.052              | 1.36               |
| Expt. (Ref. 20) | 0.2         | 0.1                | 0.12               |
|                 | 0.2         | 0.2                | 0.25               |
|                 | 0.2         | 0.5                | 0.62               |
| Expt. (Ref. 29) | 0.002       | $4 \times 10^{-5}$ | $5 \times 10^{-7}$ |
|                 | 0.08        | 0.002              | 0.001              |

large system size is required to study these defects in simulations in order to correctly simulate the long-range deformations these defects cause in the crystals. Hard spheres cannot be treated exactly using conventional BD simulations as the particles only interact during the instant they collide. This instant will always be missed in conventional BD simulations, where the forces between the particles are only evaluated at discrete time intervals. Therefore, a very steep, but finite interaction potential is usually used to model colloids. Unfortunately, a very small step size is required to accurately integrate the resulting equations of motion, which slows down the simulations. Therefore, the system sizes of interest (hundreds of thousands of particles) cannot be simulated using conventional Brownian dynamics techniques.

Molecular dynamics (MD) of hard spheres are possible using event driven simulations. In these simulations the equations of motion are integrated exactly, which is only possible because the particles exhibit free motion in between collisions and the collisions occur instantly and, therefore, only involve two particles. Therefore, we used an event driven BD simulation very similar to the techniques employed by Strating and Scala *et al.*<sup>56,57</sup> We adjust the conventional event driven MD simulations by randomly adjusting the velocities of the particles at regular intervals  $\Delta t$ . This randomization, which is similar to the velocity adjustment of an Anderson thermostat, reads

$$\mathbf{v}(t + \Delta t) = \alpha_t \mathbf{v}(t) + \beta_t \mathbf{v}_R(t), \quad (4)$$

where  $\mathbf{v}_R(t)$  is a random uncorrelated three-dimensional (3D) Gaussian variable with mean 0 and variance  $k_B T/m$ . Furthermore,  $\alpha_t$  is  $\alpha_0$  with probability  $\nu \Delta t$  and 1 otherwise. It can be shown that setting  $\beta_t = \sqrt{1 - \alpha_t^2}$  keeps the temperature constant. Finally,  $\nu$  is similar to the collision frequency of an Anderson thermostat. The velocity adjustment equation (4) together with the usual position and velocity updates of an event driven MD simulation define event-driven Brownian dynam-

ics (EDBD). Previous versions of EDBD,<sup>56,57</sup> are obtained if  $\alpha_0$  and  $\nu \Delta t$  are set to one.

Our version of event driven BD mimics Langevin dynamics with friction factor  $\gamma = (1 - \langle \alpha_t \rangle) / \Delta t$  for small  $\gamma \Delta t$ . The motion of a single particle with no forces other than these velocity adjustments can be integrated analytically to obtain the mean square displacement, and the corresponding diffusion constant reads

$$D = \langle \Delta r(t)^2 \rangle / (2t) = \frac{k_B T}{m} \frac{1 - \gamma \Delta t / 2}{\gamma}, \quad (5)$$

which has the correct value for a friction constant  $\gamma$  apart from the factor  $1 - \gamma \Delta t / 2$  which is almost unity for small  $\gamma \Delta t$ . The drift velocity  $v_d$ , when a gravitational acceleration  $g$  is applied, can also be calculated and the corresponding Peclet number reads

$$Pe_\sigma = \frac{v_d \sigma}{D} = \frac{1}{1 - \gamma \Delta t / 2} \frac{mg\sigma}{k_B T}, \quad (6)$$

which differs from the usual value by  $1/(1 - \gamma \Delta t)$ , due to the presence of this factor in the diffusion constant.

The values  $\nu = 10\tau_{MD}^{-1}$ ,  $\Delta t = 0.01\tau_{MD}$ , and  $\alpha_0 = \beta_0 = 1/\sqrt{2}$  are used in all our simulations, where  $\tau_{MD}$  is the natural time unit of an event driven MD simulation, such that  $m\sigma^2/\tau_{MD}^2 = k_B T$ . Inserting these values into the definition of  $\gamma$ ,  $\gamma \Delta t = 1 - \langle \alpha_t \rangle = \Delta t \nu (1 - \alpha_0) = 0.1(1 - 1/\sqrt{2}) \simeq 0.0293$ , which is indeed considerably smaller than 1, showing that our event driven BD approximates Langevin dynamics well. The Peclet number for our system is  $\sim Pe_\sigma = 1.015$ . The Brownian time reads

$$\tau_B = \frac{\sigma^2}{6D} \simeq 0.495\tau_{MD}. \quad (7)$$

The Brownian time  $\tau_B$  will be used as a unit of time throughout this work.

Unfortunately, the particles in our event driven Brownian dynamics simulations, like in the Langevin dynamics simulations they resemble, have finite inertia, which is a disadvantage when simulating colloids that do not have significant inertia. The inertia in our simulations most clearly shows up in the self-diffusion for large packing fractions, which does not show diffusive behavior at very short times, since the ‘‘collisions’’ with the thermostat are almost always preceded by a particle–particle collision. However, we do not expect the effects of this finite inertia to have a large effect on our results for the following reasons: (i) The initial packing fraction is chosen to be small, such that during the sedimentation stage the colloids have a large mean free path and do show diffusive behavior in between collisions. (ii) By comparing with equilibrium Monte Carlo simulations, we show that the sediment is always in quasi-equilibrium during the crystallization stage, such that the exact details of the short time dynamics are not important. For the same reasons, we do not expect hydrodynamics to play a large role in an experiment with a similar setup as our simulations (except for slowing down the diffusion in the sediment, which is taken into account in definition (2) of the dimensionless flux  $J$ ). In summary, we developed a new simulation technique, event driven Brownian dynamics simulations, which has the (in our case, slight) disadvantage of finite inertia, but which is also the only available

simulation technique that combines diffusive dynamics with the ability to simulate systems of hundreds of thousands of particles.

## D. Order parameters

We use a large set of order parameters to find the stacking and to automatically identify slanted stacking faults and (100) oriented crystals, that is, fcc domains whose (100), (010), or (001) plane is aligned with the bottom wall. However, all of these order parameters are well studied in the literature and we refer to the corresponding references for the analysis of their performance. We checked the performance of several order parameters and identified the ones that allow us to analyze the stacking, the slanted stacking faults, and the orientation of the fcc domains in crystalline sediments of hard spheres. We will define the order parameters we use and our values for the adjustable parameters that feature in their definitions. In the calculation of the 3D bond order parameter, a list of “neighbors” is determined for each particle. The neighbors of particle  $i$  include all particles within a radial distance  $r_c = 1.3\sigma$  of particle  $i$ , and the total number of neighbors is denoted by  $N_b(i)$ . An (un-normalized) bond order parameter  $q_{l,m}^u(i)$  for each particle is then defined as

$$q_{l,m}^u(i) = \frac{1}{N_b(i)} \sum_{j=1}^{N_b(i)} Y_{l,m}(\theta_{i,j}, \phi_{i,j}), \quad (8)$$

where  $\theta_{i,j}$  and  $\phi_{i,j}$  are the inclination and azimuth of the bond between  $i$  and  $j$  and  $Y_{l,m}(\theta, \phi)$  are the spherical harmonics with  $m \in [-l, l]$ . The normalized bond order parameters are defined as

$$q_{l,m}(i) \equiv q_{l,m}^u(i) / \left( \sum_{m=-l}^l |q_{l,m}^u(i)|^2 \right)^{1/2}. \quad (9)$$

Solid-like particles are identified<sup>58</sup> as particles for which the number of crystalline connections per particle  $n_{\text{con}}(i)$  is greater than a critical number  $n_c = 4$ . A neighbor  $j$  of particle  $i$  forms a crystalline connection with  $i$ , if  $d_6(i, j) > d_c$ , where the symmetry index  $l$  is chosen to be 6,  $d_c = 0.7$  is a threshold value, and  $d_l(i, j)$  is the correlation between the bond orientational order of particle  $i$  and  $j$  given by

$$d_l(i, j) = \sum_{m=-l}^l q_{l,m}(i) q_{l,m}^*(j). \quad (10)$$

In order to determine the stacking of the crystalline layers we first need to locate the hexagonal layers. To this end we measure the  $n$ -fold two-dimensional bond order parameter  $\psi_m^S(i)$  of particle  $i$  in its environment of type  $S$  (see below), defined as

$$\psi_m^S(i) = \frac{1}{N(i)} \sum_{j=1}^{N(i)} \exp(mi\theta_{ij}), \quad (11)$$

where the sum over  $j$  is over the  $N(i)$  particles in the environment (of type  $S$ ) of particle  $i$ ,  $\theta_{ij}$  is the angle between the projection of  $\mathbf{r}_{ij} \equiv \mathbf{r}_i - \mathbf{r}_j$  on the horizontal plane and

some arbitrary horizontal axis, and  $i$  (without dot) is the imaginary number. The environment for  $\psi_m^{\text{layer}}(i)$  is defined by the nearest neighbors  $j$  in the same layer, for which  $|z_j - z_i| < 0.5\sigma$  and the horizontal distance  $\rho_{ij}$  between  $i$  and  $j$  is less than  $r_c = 1.3\sigma$ . We use the hexagonal order parameter  $\psi_6(i) \equiv |\psi_6^{\text{layer}}(i)|$  to determine the crystalline order within a horizontal layer. The environment of a solid-like particle  $i$  is hexagonal ordered in the plane perpendicular to gravity, if  $\psi_6(i) > 0.7$ . The stacking can only be defined if the neighbors in the layer above and below  $i$  are hexagonally ordered and are a part of the same crystalline domain. This is defined to be the case if  $\psi_6^{\text{stair}}(i) \equiv |\psi_6^+(i) + \psi_6^-(i)| > 0.5$  with  $\psi_6^S(i)$  being the hexagonal order parameter of particle  $i$ . Here  $S = +$  corresponds to the neighbors  $j$  in the layer above particle  $i$ , for which  $0.55\sigma < (z_j - z_i) < 1.2\sigma$  and  $\rho_{ij} < 0.95\sigma$ , while  $S = -$  corresponds to the neighbors in the layer below  $i$ , for which  $-1.2\sigma < (z_j - z_i) < -0.55\sigma$  and  $\rho_{ij} < 0.95\sigma$ . Note that there are particles  $j$  with  $0.5\sigma < |z_j - z_i| < 0.55\sigma$ , which are excluded from the calculation of both  $\psi_m^{\text{layer}}(i)$  and  $\psi_m^{\pm}(i)$ . However, the number of excluded particles is very small, as the region  $0.5\sigma < |z_j - z_i| < 0.55\sigma$  is only  $0.05\sigma$  thick and will most of the times be located in between the layers, where the density is small.

To determine the stacking of the hexagonal layers we use the trigonal bond order parameter of particle  $i$ ,  $\psi_3^S(i)$ , where the neighbors corresponding to  $S = \pm$  are defined analogously to  $\psi_6^S(i)$ . For perfect fcc,  $\psi_3^{\text{fcc}}(i) \equiv |\psi_3^+(i) + \psi_3^-(i)| = 1$ , while  $\psi_3^{\text{hcp}}(i) \equiv |\psi_3^+(i) - \psi_3^-(i)| = 1$  for perfect hcp. The stacking parameter  $\alpha(i) \equiv \psi_3^{\text{fcc}}(i) / [\psi_3^{\text{fcc}}(i) + \psi_3^{\text{hcp}}(i)]$  measures whether particles are fcc or hcp stacked. Particle  $i$  belongs to a (111) oriented fcc domain if  $\alpha(i) > 0.5$  and to a hcp domain otherwise.

In order to identify the stacking faults, we use the average local bond order parameters  $\bar{w}_l(i)$ . Following Lechner *et al.*,<sup>59</sup> a crystalline particle  $i$  is identified as fcc stacked when  $\bar{w}_4(i) > \bar{w}_c$  and hcp stacked otherwise. Here,  $\bar{w}_l(i)$  is defined as

$$\bar{w}_l(i) = \sum_{m_1, m_2, m_3} \begin{pmatrix} l & l & l \\ m_1 & m_2 & m_3 \end{pmatrix} \bar{q}_{l, m_1}(i) \bar{q}_{l, m_2}(i) \bar{q}_{l, m_3}(i) \quad (12)$$

with  $\begin{pmatrix} l & l & l \\ m_1 & m_2 & m_3 \end{pmatrix}$  being the Wigner  $3j$  symbols, the sums over  $m_1, m_2$ , and  $m_3$  run over all values between  $-l$  and  $l$  such that  $m_1 + m_2 + m_3 = 0$ , and

$$\bar{q}_{l,m}^u(i) = \frac{1}{\bar{N}_b(i)} \sum_{k=1}^{\bar{N}_b(i)} q_{l,m}^u(k). \quad (13)$$

The sum over  $k$  denotes a sum over the neighbors of particle  $i$  including the particle itself. We use the threshold value  $\bar{w}_c = -0.07$ . Finally,  $\bar{q}_{l,m}^u(i)$  are normalized using Eq. (9). In principle, this parameter could also be used to define the stacking of the horizontal layers. However, this might lead to a bias towards either fcc or hcp, when threshold  $\bar{w}_c$  is not chosen exactly right. The definition of  $\alpha(i)$  using  $\psi_3^{\text{fcc}}(i)$  and  $\psi_3^{\text{hcp}}(i)$  as described above, has no such threshold value and is guaranteed to lead to  $\alpha = 0.5$  for a crystal with perfectly random stacking. Furthermore, the distribution of  $\alpha(i)$  (not shown) for the particles that are (111) fcc or hcp has

TABLE II. The various structures observed in the crystalline sediment and the criteria on the order parameters that we use to find particles that belong to such structures. The various symbols are explained in the text.

| Structure                        | Conditions on particle $i$   |
|----------------------------------|--|
| Crystalline                      | $n_{\text{con}}(i) > 4$  |
| (111) oriented fcc               | $n_{\text{con}}(i) > 4$ , $\psi_6(i) > 0.7$ , $\psi_6^{\text{Surr}}(i) > 0.5$ , and $\alpha(i) > 0.5$    |
| Hcp                              | $n_{\text{con}}(i) > 4$ , $\psi_6(i) > 0.7$ , $\psi_6^{\text{Surr}}(i) > 0.5$ , except $\alpha(i) < 0.5$ |
| Slanted stacking fault candidate | $n_{\text{con}}(i) > 4$ , $\psi_6(i) < 0.7$ , $\bar{w}_4(i) > -0.07$                                     |
| Slanted stacking fault           | $i$ is a slanted stacking fault candidate and $n_{\text{st}}(i) \geq 4$                                  |
| (100) oriented fcc               | $n_{\text{con}}(i) > 4$ , $\bar{w}_4(i) \leq -0.07$ , $\psi_6(i) < 0.7$ , and $\psi_4(i) > 0.5$          |

two clearly separated peaks, (corresponding to fcc and hcp) with a density of  $\alpha(i)$  values that is nearly zero in between. Finally, we also identify (100) oriented fcc domains by  $\bar{w}_4(i) \leq -0.07$ ,  $\psi_6(i) < 0.7$ , and  $\psi_4(i) > 0.5$ .

In Table II, we list the structures which our analysis finds and the corresponding conditions on the order parameters. By definition, defect structures have limited crystalline order and, consequently, they are hard to detect by crystalline order parameters. For this reason, particles are occasionally misidentified as part of a slanted stacking fault, especially near the crystal–fluid interface. Therefore, we first define for all particles, whether or not they are a slanted stacking fault candidate as defined in Table II. Subsequently, a stacking fault candidate  $i$  is defined to be part of a slanted stacking fault, if it has more than a certain number of neighbors that are also slanted stacking fault candidates; we denote the number of such neighbors by  $n_{\text{st}}(i)$ . With this modification, the identification of the various defect features is surprisingly accurate.

### III. RESULTS AND DISCUSSION

We performed five separate EDBD runs of  $N = 4 \times 10^5$  particles with varying initial volume fractions. First, we will discuss the results for the lowest volume fraction  $\phi_i \simeq 0.01$  and subsequently we will discuss the effect of volume fraction on our results. In this entire work, the gravitational length  $\ell$  is set to  $\sigma$  ( $\text{Pe}_\sigma \simeq 1$ ).

We show the onset of crystallization and the final configuration of the crystal as observed during these runs with the aid of typical snapshots in Fig. 1.<sup>60</sup> The particles are colored

depending on whether a particle is a part of a fcc or hcp crystal, or a slanted stacking fault, which is determined using the methods described in Sec. II D. At first, particles that have sedimented onto the bottom wall form a fluid that becomes increasingly dense due to the increasing gravitational pressure. Once the pressure due to the gravitational push of particles in the sediment reaches the crystallization pressure, the system starts to crystallize. Just after the crystallization of the first layers, the fluid–crystal interface can be seen to be very rough in Fig. 1(a), with small piles of crystalline particles in an otherwise disordered fluid phase. The roughness of this interface is still visible when the sedimentation is completed, see Fig. 1(b). Clearly, fcc particles, which are color-coded green in Fig. 1, occur predominantly in the final configuration. More quantitative information about the stacking of the layers in the final configuration can be found in Fig. 2, where the stacking parameter  $\alpha_n = N_n^{\text{fcc}}/N_n^{\text{stack}}$  of layer  $n$  is shown, which is equal to the number of fcc particles  $N_n^{\text{fcc}}$  in layer  $n$  divided by the total number of particles  $N_n^{\text{stack}} = N_n^{\text{fcc}} + N_n^{\text{hcp}}$  in layer  $n$  for which the stacking could be defined. The stacking parameter was averaged over five runs to obtain sufficient statistics. In the experiments of Hoogenboom *et al.*<sup>19</sup> and a previous simulation study,<sup>21</sup> it is shown that the local osmotic pressure at which the first layer crystallizes is larger than the local osmotic pressure at crystallization of the other layers. Therefore, the crystallization of the second and third layer occur before the first layer is fully formed. For this reason, the first few layers are not well-equilibrated, which presumably explains the small value of  $\alpha_n$  for the first few layers  $n$  in Fig. 2, which was also observed in experiments.<sup>28</sup> For our

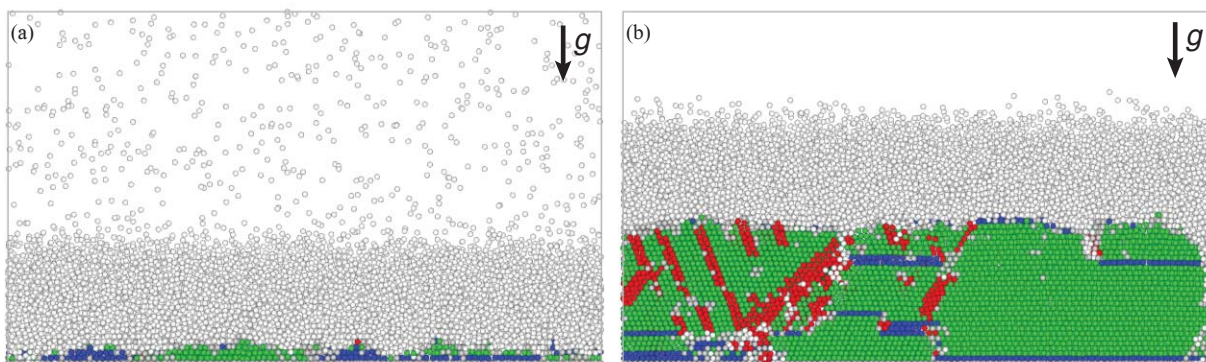


FIG. 1. The side view of the sediment just after crystallization at  $t = 4441\tau_B$  (a) and at the end of the simulation,  $t = 13928\tau_B$ . The direction of gravity is denoted by the arrow labeled “g.” The colors denote the stacking (light green: fcc, blue: hcp) and the defects (white: disordered/fluid, red: slanted stacking fault, dark green: (100) oriented fcc). Gray particles are ordered, but the stacking could not be defined (see Sec. II D).

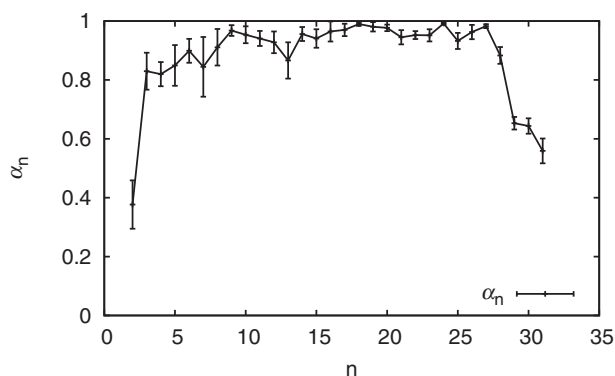


FIG. 2. The fraction of (111) oriented fcc particles  $\alpha_n \equiv N_n^{\text{fcc}}/N_n^{\text{stack}}$  in layer  $n$  as a function of  $n$ , where  $N_n^{\text{fcc}}$  is the number of fcc-like particles (see Sec. II D) and  $N_n^{\text{stack}}$  is the number of particles in layer  $n$  for which the stacking could be measured. The first layer is absent because no stacking parameter  $\alpha_n$  can be defined for  $n = 1$ .

simulations, the third layer seems relatively well equilibrated in that respect, since the stacking parameter  $\alpha_3$  is large. However, the third layer of the sediment of Hoogenboom *et al.*<sup>28</sup> was not predominantly fcc stacked, which might be explained by the hydrodynamic interactions between the wall and the colloids, which slow down the diffusion. We will focus on the fourth layer and higher, in order to enable comparison with experiments.

In Fig. 3, we show typical snapshots during the crystallization and subsequent equilibration of the fourth layer. Small crystallites form at first, as also visible from Fig. 1, which are randomly stacked. When the crystallites grow larger, more of these crystallites are found to be fcc stacked. The horizontal growth of the crystallites proceeds until they meet, at the time when a poly-crystalline sediment of a few layers is formed. The smaller of the crystalline domains in these layers slowly disappear, while the larger remain and typically define the domains in the layers above. Further rearrangements are only possible after very long times. Interestingly, these rearrangements sometimes result in the appearance of (100) oriented fcc crystallites, while a simple calculation shows that the (111) oriented crystallites result in a lower free energy, because the gravitational energy of the (111) crystallites is lower, and the interfacial tension between a fcc crystal and a hard wall is lowest if the (111) face of fcc is at the wall.<sup>61</sup> We observed that these (100) oriented crystallites typically originate at grain boundaries where two or three crystallites meet that have sufficiently incompatible lattice directions. One of the horizontal lattice directions of the (100) is always aligned with one of the original crystallites, while the other one is usually aligned with one of the other original crystallites, see Fig. 3. In this way, the (100) crystallites help to relieve stresses on the interface between crystallites with misaligned lattice directions.

### A. Slanted stacking faults

Crystalline sediments of colloids usually contain many defects, such as vacancies and grain boundaries. The most striking defects are formed when, on top of a hexagonal do-

main with horizontal position A, two different domains grow, for which particles occupy the B and C positions as depicted in Fig. 4. Where these two domains meet, a (straight) line of holes is formed, which are too small to fit a particle in. The next layer can be A stacked, in which case the defect is covered over. The resulting line defect, due to ACA and ABA stacked domains, can diffuse relatively easily and will likely merge with another line defect (or grain boundary). Other possibilities are ACA and ABC. In principle, ACB and ABC are also possible, but this causes a wide line defect which is unfavorable.<sup>53</sup> Hilhorst *et al.* argued that the defect line of holes will be partially filled with particles due to the gravitational force on these particles. The configuration of the particles around the line defect causes these particles to be ACA and ABC stacked.<sup>20</sup> Therefore, the ACA and ABA scenario is unlikely. Similarly, the defect will also persist in the next layers, forcing the stacking of both crystallites to be fcc. Such a process results in planar defects along one of the  $(\bar{1}\bar{1}1)$ ,  $(\bar{1}1\bar{1})$ , and  $(11\bar{1})$  planes, if the plane of the fcc crystal aligned with the bottom wall is (111). When such a planar defect is shifted perpendicular to the plane of the defect, such that the gap between the hexagonal layers on either side of the defect is closed, a stacking fault (consisting of two hcp layers) is formed (see Fig. 4). Stacking faults occur frequently in atomic fcc crystals<sup>22</sup> and are most likely also the planar defects that cost the least free energy (per unit area) in hard-sphere crystals. Because the stacking faults are slanted with respect to the bottom wall in our case, they are called slanted stacking faults. The shift that closes the aforementioned gap results in a vertical displacement between the two horizontal domains of about one third of a diameter.<sup>20</sup> In practice, the vertical shift starts out being zero at the originating line defect (the gap between the B and C stacked domains) and it increases slowly to  $\sigma/3$  as the slanted stacking fault grows. Once this vertical shift is formed, the formation of a single horizontal domain that covers the defect is complicated further. In this case, fcc continues to grow on both sides of the slanted stacking fault (in a direction parallel to the stacking fault).<sup>53</sup> It is suggested that this effect explains the occurrence of fcc in colloidal sediments.<sup>20</sup>

The configurations in Figs. 1 and 3, show clearly that the slanted stacking faults are the most common defects. If slanted stacking faults indeed force the stacking to be fcc, one should observe an increase in fcc after the number of slanted stacking faults has increased. To investigate the order of these two events, we show the behavior of the stacking parameter  $\alpha_n$  and the fraction of particles that are part of a stacking fault as a function of time in Fig. 5 for two individual layers  $n = 4$  and  $n = 15$ . The fourth layer forms fcc domains quite rapidly as shown in Fig. 5, while the slanted stacking faults take longer to fully develop. This is the case for all layers  $3 < n \lesssim 8$ . For these layers we do not expect the slanted stacking faults to play a major role in determining the stacking. However, for the layers  $n \gtrsim 9$ , large slanted stacking faults emerge during or immediately after the crystallization, probably due to the presence of slanted stacking faults in the layers below. The stacking parameter  $\alpha_n$  of layer  $n$  also increases at the same time and, therefore, we are not certain that the larger value of  $\alpha_n$  is caused by the slanted stacking faults.

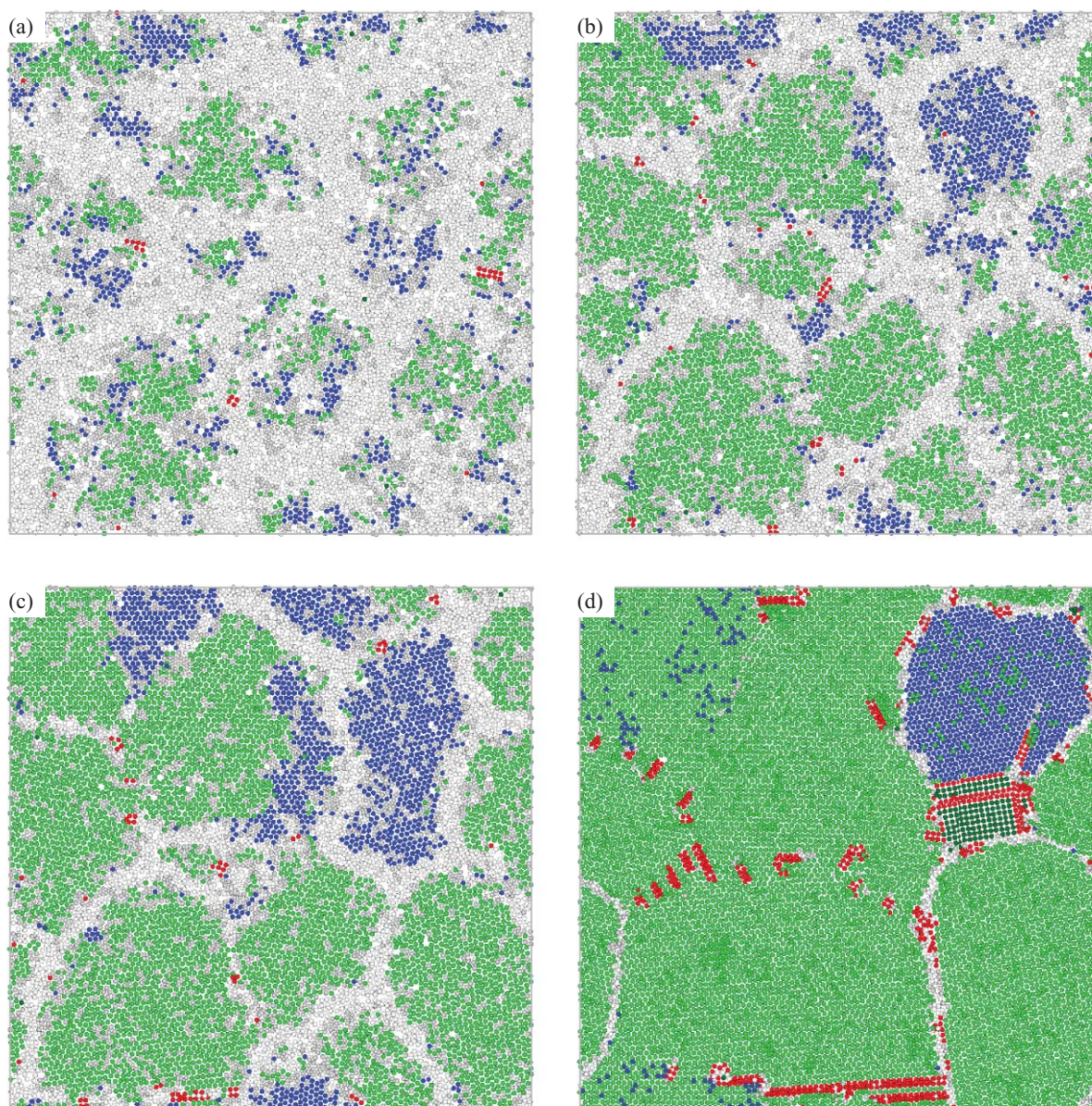


FIG. 3. The fourth layer (from the bottom) for different times  $t/\tau_B = 4441$  (a), 4643 (b), 4844 (c), and 13928 (d). Gravity is directed into the plane of the figure. The colors are the same as in Fig. 1.

We notice that more slanted stacking faults in the lower layers form at longer times, see Fig. 5. This cannot be explained by nucleation on a layer which has two adjacent domains which are stacked differently, since the domains do not change anymore. We postulate that these slanted stacking faults are formed to relieve the stress caused by the decrease of the (gravitational) pressure with height in the sediment. The lower layers form with a lattice constant close to the coexistence value. However, the pressure on a layer increases due to the increasing number of layers on top, which should result in a smaller lattice constant of this layer. However, a smaller lattice constant is incompatible with the lattice of the layers above. To resolve the incompatibility of lattice constants, slanted stacking faults will be formed, as has been shown by Schall *et al.* by sediment-

ing colloidal hard spheres on an ill-fitting template.<sup>45</sup> In a Monte Carlo simulation of an initially perfect fcc crystal with a lattice constant of  $1.1\sigma$ , around the coexistence value, slanted stacking faults were also found (not shown). However, a simulation with a lattice constant of  $1.06\sigma$ , a more reasonable lattice constant for the pressure at the bottom (around  $40k_B T \sigma^{-3}$ ),<sup>21</sup> did not show these defects. This shows that slanted stacking faults can indeed form in order to relieve stress, when part of a crystal becomes denser than the rest of the crystal. Finally, crystallites with similar lattice directions sometimes formed a single crystallite by slowly changing lattice directions and the resulting stress was also relieved with the aid of short slanted stacking faults perpendicular to the interface between the original crystallites.

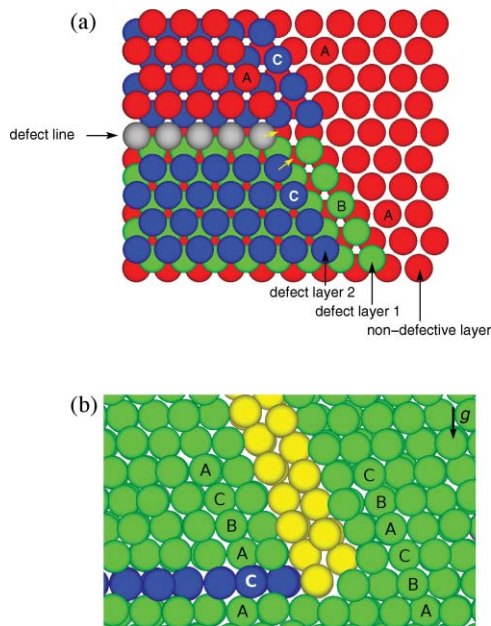


FIG. 4. (a) Top view of the origin of a slanted stacking fault (idealized): when a B stacked domain (green) and a C stacked domain (blue) grows on top of a single A domain (red), a line defect is formed (as indicated). A line of particles (gray) on top of the defect have a lower  $z$ -position (the direction of gravity (opposite to the  $z$  direction) points into the plane). To avoid overlap with the gray particles, only a C domain can grow on top of the B domain. The defect in the top layer can be healed by slightly shifting the gray particles and the particles in the C domain (as indicated by the yellow arrows). (b) Side view of a slanted stacking fault observed in an EDBD simulation: the slanted stacking fault in yellow; fcc stacked particles are colored green, hcp stacked particles are colored blue. No stacking can be defined for the first layer (A); it is colored arbitrarily green. The hexagonal layers are oriented perpendicular to the direction of gravity (as denoted by the arrow labeled “ $g$ ”).

## B. Explanation of the stacking behavior

As we were unable to show that there is a link between slanted stacking faults and the stacking parameter  $\alpha_n$ , we propose an alternative explanation for the high values of  $\alpha$ . Our explanation is based on the free energy difference between fcc and hcp and therefore assumes that the system is locally in thermodynamic equilibrium. Since the particle flux

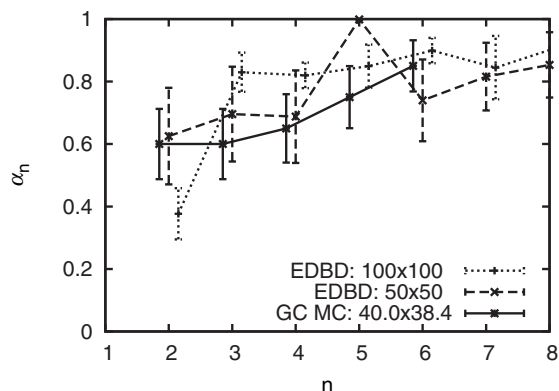


FIG. 6. The stacking parameter  $\alpha_n$  as a function of the layer number  $n$ . The results from event driven Brownian dynamics simulations (EDBD) with horizontal box sizes of  $50\sigma \times 50\sigma$  (dashed line) and  $100\sigma \times 100\sigma$  (dotted line) are compared to grand canonical Monte Carlo simulations with horizontal box size  $40\sigma \times 38.4\sigma$  (solid line). Small horizontal shifts are applied to the points to allow easier distinction between them.

$J \simeq 0.104$  in our simulations is not much smaller than the one for the EDBD simulations, particles might not have sufficient time to rearrange and reach local equilibrium. In order to check whether or not our EDBD simulations correspond with (near) thermodynamic equilibrium conditions, we perform grand canonical MC simulations, in which a thin sedimentary crystal is grown essentially infinitely slowly. In addition, the thickness of the crystalline part of the sediment is limited to 7 layers, so that stresses due to the pressure differences play hardly any role. Hence, the crystalline sediments obtained from MC simulations, where no slanted stacking faults are formed, can be regarded as well-equilibrated. We note that the system sizes of the MC simulations are much larger than in Ref. 21, but still considerably smaller than in the EDBD simulations as the MC simulations are less efficient than our EDBD simulations. We compare the stacking parameter  $\alpha_n$  obtained from MC simulations to the results from EDBD simulations with a horizontal box size of  $100\sigma \times 100\sigma$  and  $50\sigma \times 50\sigma$  and with the same initial volume fraction in Fig. 6. The size of the crystal in the Monte Carlo simulations was equal to the horizontal box size, which

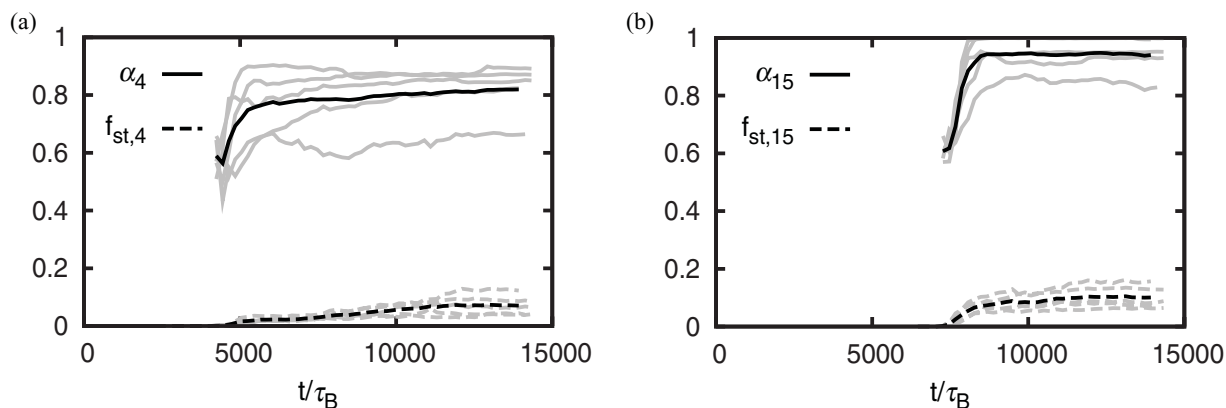


FIG. 5. The fraction of (111) oriented fcc particles  $\alpha_n \equiv N_n^{\text{fcc}}/N_n^{\text{stack}}$  and particles in a slanted stacking fault  $f_{\text{st},n} \equiv N_n^{\text{slst}}/N_n$  in layer  $n$  for  $n = 4$  (a) and  $n = 15$  (b), as a function of time  $t$ , where  $N_n^{\text{fcc}}$  is the number of fcc-like particles in layer  $n$ ,  $N_n^{\text{slst}}$  is the number of particles in a slanted stacking fault in layer  $n$ ,  $N_n^{\text{stack}}$  is the number of particles in layer  $n$  for which the stacking could be reliably determined, and  $N_n$  is the total number of particles in layer  $n$ . Shown are the averages of 5 runs (black line) as well as the results from the 5 separate runs (gray lines).

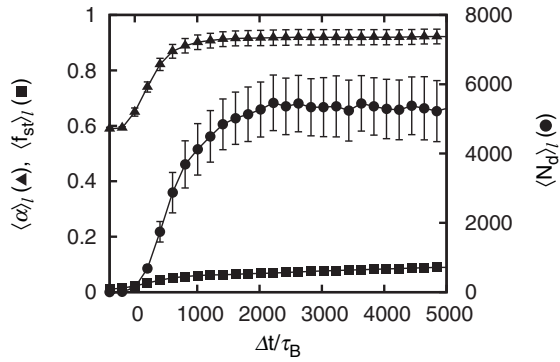


FIG. 7. The stacking parameter  $\langle \alpha \rangle_l$  (triangles; left axis), the domain size  $\langle N_d \rangle_l$  (circles; right axis), and the fraction of particles in slanted stacking faults  $\langle f_{st} \rangle_l$  (squares; left axis) of a layer for  $\phi_i = 0.01$  as a function of the amount of time  $\Delta t$  elapsed since time  $t^{50\%}$  at which 50% of the particles in a layer was crystalline. In the special average  $\langle \cdot \rangle_l$  over all layers, the property of a layer  $n$  at interest is taken from the snapshot at  $t = t_n^{50\%}$  (see text). Finally, the average and standard error for each  $\Delta t$  are calculated from five independent EDBD runs with  $4 \times 10^5$  particles.

is approximately equal to the size of the domains that grew in both EDBD simulations. The similarity between the MC and EDBD results shows that slanted stacking faults play a minor role in determining the stacking in slowly grown sediments of (colloidal) hard spheres. We propose that the fcc stacking is due to the tiny free energy per particle that is multiplied by the large number of crystalline particles in a domain. In Fig. 7, we plot the average stacking parameter  $\langle \alpha \rangle_l$ , the average domain size  $\langle N_d \rangle_l$ , and the average fraction of solid-like particles in a slanted stacking fault  $\langle f_{st} \rangle_l$  as a function of  $\Delta t$ , the time elapsed since the layer was 50% crystalline, averaged over all layers  $n$  and five EDBD runs with  $4 \times 10^5$  particles. The subscript  $l$ , denotes the average of any property  $X$  over all layers such that the time  $\Delta t$  since each layer was 50% crystalline is held fixed, *i.e.*,  $\langle X \rangle_l(\Delta t) \equiv \sum_n X_n(t_n^{50\%} + \Delta t) / N_l(\Delta t)$ , where  $X_n(t)$  is  $X$  averaged over the particles in a layer  $n$  at time  $t$ . The sum runs over the  $N_l(\Delta t)$  layers for which  $t_n^{50\%} + \Delta t < t_{\text{tot}}$ , where  $t_{\text{tot}}$  denotes the total run time. Note that this average, which measures a property at a different time for each layer, differs from  $\langle X \rangle$ , which we will use to denote the average over all crystalline layers in a single snapshot. Clearly, the average number of particles in a domain around the time that the domains become primarily fcc stacked is of the order of a few thousand, which gives a free energy difference of several  $k_B T$  for hcp and fcc, which is large enough to explain the observed preference for fcc.

This argument can be made more quantitative by comparing measured stacking sequences to a theoretical prediction. Mau and Huse<sup>48</sup> determined the free energy of various stacking sequences in bulk systems and fitted a general stacking free energy expression to their results. Their expression features the free energy of three layers, depending on the stacking  $\sigma_l$  of each layer, where  $\sigma_l = +$  if layer  $l$  is fcc stacked and  $\sigma_l = -$  if layer  $l$  is hcp stacked. Mau and Huse<sup>48</sup> showed that one of the terms in their general expression has a prefactor which is zero within the statistical error and, therefore, we will neglect this term. For a crystal grown by sedimentation, the stacking of layer  $l$  depends within reasonable approximation only on the stacking of the layers  $l-1$  ( $\sigma_{l-1}$ ) and  $l-2$

TABLE III. The probability  $P_{+|\sigma_{l-1}\sigma_{l-2}}$  to find a fcc layer (denoted by '+') on top of two layers with stacking  $\sigma_{l-2}$  and  $\sigma_{l-1}$  as measured in the final configurations of the EDBD simulations and as calculated using Eq. (15).

| $P_{\sigma_l \sigma_{l-1}\sigma_{l-2}}$ | Measured | Calculated |
|---|----------|------------|
| $P_{+ --}$                              | 0.83(13) | 0.743      |
| $P_{+ +-}$                              | 0.81(4)  | 0.852      |
| $P_{+ -+}$                              | 0.52(10) | 0.594      |
| $P_{+ ++}$                              | 0.93(1)  | 0.919      |

( $\sigma_{l-2}$ ), since the layers above  $l$  are not completely formed at the time when the stacking is determined. Using this approximation, the probability that layer  $l$  is fcc ( $\sigma_l = +$ ) rather than hcp ( $\sigma_l = -$ ) stacked, is equal to

$$P_{+|\sigma_{l-1}\sigma_{l-2}} = 1 / \{1 + \exp[-\beta \Delta F(\sigma_{l-1}, \sigma_{l-2})]\}, \quad (14)$$

where  $\Delta F(\sigma_{l-1}, \sigma_{l-2})$  is the free energy difference between the three-layer configuration that features a hcp-like layer  $l$  and the configuration with a fcc-like layer  $l$ , while the stacking of layers  $l-1$  and  $l-2$  is  $\sigma_{l-1}$  and  $\sigma_{l-2}$ , respectively, in both configurations. Using the expression of Mau *et al.*,<sup>48</sup> this free energy difference can be written as

$$\Delta F(\sigma_{l-1}, \sigma_{l-2}) = N_d [h + \sigma_{l-1} \gamma^* + \sigma_{l-2} \sigma_{l-1} h'], \quad (15)$$

where  $N_d$  is the number of particles per layer in the domain. The stacking parameters obtained by Mau *et al.*<sup>48</sup> are  $h = 74 \pm 6$ ,  $\gamma^* = 36 \pm 6$ , and  $h' = 18 \pm 6$  in units of  $10^{-5} k_B T$  at the density of the hard sphere crystal at bulk coexistence. Note that the bulk free energy difference between hcp and fcc is simply  $(h + h')$  per particle and that  $\gamma^*$  is the surface free energy per particle of the interface between a bulk fcc crystal and a bulk hcp crystal,<sup>23</sup> when the interface between the two crystals is chosen along a hexagonal plane. The corresponding interfacial tension is simply  $\gamma^*$  divided by the area per particle in a hexagonal layer. In Table III,  $P_{+|\sigma_{l-1}\sigma_{l-2}}$  averaged over all layers in the final configurations of five EDBD simulations with  $\phi_i \simeq 0.01$  is compared with the theoretical three-layer stacking probability. The only adjustable parameter in Eq. (15) is the domain size  $N_d$  at the time when the stacking is determined. Accordingly, we set  $N_d$  to 1900, the domain size at  $t - t_l^{50\%} \simeq 400\tau_B$ , when the rate of change of  $\langle \alpha_l \rangle$  is the largest. The excellent agreement between the measured and predicted stacking probabilities shows that even the smaller terms in the free energy can have a measurable effect if the typical size  $N_d$  of a domain is large enough. Furthermore, this indicates that, at least for small  $J$ , the stacking of sedimented hard sphere crystals within a single domain is completely determined by free energy effects. The values of  $h$ ,  $\gamma^*$ , and  $h'$  depend on the density of the bulk crystal<sup>48</sup> and, therefore, are susceptible to fitting. However, the deviation between the results and Eq. (14) is only 0.96 times the error averaged over the four points and the deviations can be reduced to 0.56 times the error on average by increasing  $h'$  by its standard error (*i.e.*,  $h' \rightarrow 24$ ). We conclude that the values of  $h$ ,  $\gamma^*$ , and  $h'$  at bulk coexistence describe our results well and further fitting is not justified. The main assumption in the derivation of Eq. (15) is that the time a horizontal domain requires to equilibrate is much smaller than the time it requires to grow, such that the domain is always in equilibrium while it grows.

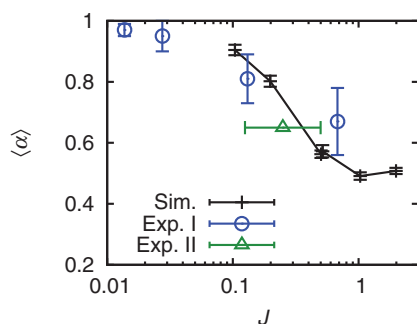


FIG. 8. The stacking parameter  $\langle \alpha \rangle$  averaged over the whole crystalline part of the final configuration from EDBD simulations with varying  $\phi_i$ , and experiments (Refs. 20 and 28) as a function of the dimensionless sedimentation flux  $J$ . The values for  $J$  are listed in Table I. The results from EDBD simulations are denoted by the pluses, while the circles and the triangle denote the experimental results of Hoogenboom *et al.* (Ref. 28) (Expt. I) and Hilhorst *et al.* (Ref. 20) (Expt. II), respectively. The simulation results at  $J \simeq 0.5$  and  $1$  lie on top of each other.

### C. Effect of initial volume fraction and sedimentation speed

In order to study the effect of the initial volume fraction  $\phi_i$ , we compare EDBD simulations with  $\phi_i = 0.02, 0.05$ , and  $0.2$  to the simulations with  $\phi_i = 0.01$  that are discussed in Secs. III A and III B of this paper. These simulations at higher volume fraction correspond to  $J$  of the order of  $1$ , see Table I, that is, the effect of the limited equilibration time is expected to become significant. Furthermore, these values for  $J$  are similar to the ones in the experiments of Hilhorst *et al.*<sup>20</sup> The observed average stacking parameters  $\langle \alpha \rangle$  in our EDBD simulations are compared to experimental results in Fig. 8. The trend in the dependence of  $\alpha$  on  $J$  is the same for experiments and simulations: the fcc stacking parameter  $\langle \alpha \rangle$  decreases with  $J$  (and thus with volume fraction  $\phi_i$ ). Quantitative agreement within the error bars of the experiments can even be found, providing confidence in our simulation method. All EDBD simulations are performed with the same number of particles and gravitational length. Therefore, the stress in the crystal caused by the increasing gravitational pressure with decreasing height in the sediment, which has been quoted to have an effect on sedimented crystals,<sup>36,38</sup> is the same in all cases. Figure 9 shows the final configuration of the fourth layer for  $\phi_i = 0.2$ , which we compare with the one for  $\phi_i = 0.01$  as displayed in the bottom right panel of Fig. 3. The most striking difference is the much smaller size of the ordered domains for  $\phi_i = 0.2$  than for  $\phi_i = 0.01$ . The decrease in domain size with increasing  $J$  causes a decrease in the free energy difference between the fcc and hcp stacking of a domain (Eq. (15)), which might explain the observed decrease in fcc stacking. However, at these high volume fractions, the free energy difference might not be the dominant factor. Another likely reason for the more random stacking in the simulations with a higher initial volume fraction is that the layers simply have less time to sample phase space and find their equilibrium structure.

Hilhorst *et al.*<sup>20</sup> showed that the probability  $P_{\text{hf}}$  to form a fcc layer on top of a hcp layer depended on the average stacking probability  $\langle \alpha \rangle$  in a crystallite in a way that could

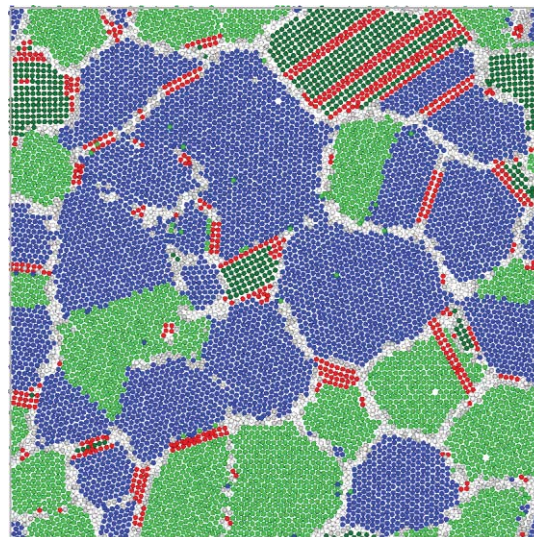


FIG. 9. The fourth layer (from the bottom) of the final configuration of an EDBD simulation at  $\phi_i = 0.2$ . The color-coding is the same as in Fig. 3. Gravity is directed into the plane of the paper.

neither be explained by the free energy difference between fcc and hcp, nor by the surface tension between the two. The model that did give a good fit to the data assumes that randomly stacked crystallites co-existed with primarily fcc-like crystallites. The authors postulated that the fcc growth of the domains is caused by a slanted stacking fault. We indeed find the presence of slanted stacking faults in some of the fcc domains in Figs. 3 and 9. However, an alternative explanation for the difference in stacking of the various crystalline domains is as follows. The spread of domain sizes in the sample is quite large, as can be seen from Figs. 3 and 9. As a consequence, there will be domains both smaller and larger than the critical domain size for which the free energy difference between the fcc and hcp stacking starts to become significant (about 1000 particles). Since the dependence of the stacking probability is exponential in the domain size, the larger domains will have a considerably larger probability to be fcc stacked than the smaller domains. It is interesting to investigate the domain size distribution and the different domains in more detail in future experiments and simulations.

Finally, we also lowered the sedimentation velocity, by decreasing the Peclet number. This should have a negative effect on both mechanisms for the formation of slanted stacking faults that were described in Sec. III A. Indeed, we find a significant decrease (about a factor of four) in the number of slanted stacking faults (not shown), when the Peclet number is decreased from  $1.015$  to  $0.5008$  at a constant  $J$  of about  $0.5$ . However, the corresponding stacking probabilities are the same within the error bounds, see Fig. 8. This provides further evidence that the slanted stacking faults are not the main cause of the preference for fcc.

## IV. CONCLUSIONS

We have employed a new simulation method to study the crystallization dynamics of sedimenting hard spheres. This method is based on event driven MD simulations which is

extended to include Brownian dynamics. Our results show that primarily fcc-stacked crystals are grown instead of randomly stacked crystals, if the Peclet number is not too high and the initial configuration is a low density homogeneous fluid phase. These findings are in agreement with experiments.<sup>28</sup> Similar defect structures as in other experiments<sup>20,53</sup> were found, among which were the slanted stacking faults along a hexagonal plane of fcc other than the plane which is aligned with the wall. The observation of Hilhorst *et al.*<sup>20</sup> that slanted stacking faults cause an increased preference for fcc could not be confirmed using our simulations. Although we did find a correlation between slanted stacking faults and a preference for fcc, this correlation is expected since the slanted stacking faults can only form and persist in fcc regions. As an explanation for the large amount of fcc found in our simulations, we propose that the preference for fcc can be explained simply by the equilibrium free energy difference between fcc and hcp, which can be larger than the thermal energy for large domains ( $\gtrsim 1000$  particles). All results observed by Hilhorst *et al.*,<sup>20</sup> which seemed to indicate the role of slanted stacking faults in determining the stacking can also be explained by free energy expressions and taking a distribution of domain sizes into account. We thus assume that the system is (nearly) in thermodynamic equilibrium, which can only be true if the top layer of a crystalline domain has sufficient time to equilibrate.

We have shown that the dimensionless particle flux  $J$ , proportional to the initial volume fraction and the sedimentation speed, is an excellent tool for gauging the extent to which the sedimentation disturbs the equilibrium. In our simulations with varying initial volume fractions and sedimentation speeds, as well as in experiments,<sup>20,28,29</sup> randomly stacked crystals were found when  $J$  was larger than 0.5, while a clear preference for fcc was found when  $J$  was less than 0.2. We should note that it is not proven that slanted stacking faults have no effect on the stacking at all although we could not measure any effect in our simulations. Furthermore, slanted stacking faults might prove important for processes, which are too slow to measure in our simulations, such as the conversion of the rhcp crystal to fcc.<sup>23,32</sup> Finally, we note that our arguments based on free energies can only explain the stacking of crystals that are grown layer by layer at a wall. This excludes experiments with volume fractions above coexistence and/or with Peclet numbers which are very small.<sup>54</sup>

## ACKNOWLEDGMENTS

Financial support is acknowledged from an NWO-VICI grant and from the High Potential Programme of Utrecht University. We are grateful to J. Hilhorst and A. van Blaaderen for useful discussions.

<sup>1</sup>W. W. Wood and J. D. Jacobson, *J. Chem. Phys.* **27**, 1207 (1957).

<sup>2</sup>B. J. Alder and T. E. Wainwright, *J. Chem. Phys.* **27**, 1208 (1957).

<sup>3</sup>W. G. Hoover and F. H. Ree, *J. Chem. Phys.* **49**, 3609 (1968).

<sup>4</sup>P. G. Bolhuis, D. Frenkel, S. C. Mau, and D. A. Huse, *Nature (London)* **388**, 235 (1997).

<sup>5</sup>S. Auer and D. Frenkel, *Nature (London)* **409**, 1020 (2001).

<sup>6</sup>B. O'Malley and I. Snook, *Phys. Rev. Lett.* **90**, 085702 (2003).

<sup>7</sup>P. N. Pusey and W. van Megen, *Nature (London)* **320**, 340 (1986).

<sup>8</sup>A. Yethiraj and A. van Blaaderen, *Nature (London)* **421**, 513 (2003).

<sup>9</sup>R. Piazza, T. Bellini, and V. Degiorgio, *Phys. Rev. Lett.* **71**, 4267 (1993).

<sup>10</sup>M. A. Rutgers, J. H. Dunsmuir, J.-Z. Xue, W. B. Russel, and P. M. Chaikin, *Phys. Rev. B* **53**, 5043 (1996).

<sup>11</sup>T. Biben, J. P. Hansen, and J. L. Barrat, *J. Chem. Phys.* **98**, 7330 (1993).

<sup>12</sup>T. Biben, R. Ohnesorge, and H. Löwen, *Europhys. Lett.* **28**, 665 (1994).

<sup>13</sup>D. C. Hong, *Phys. A* **271**, 192 (1999).

<sup>14</sup>J. A. Both and D. C. Hong, *Phys. Rev. E* **64**, 061105 (2001).

<sup>15</sup>W. Nuesser and H. Versmold, *Mol. Phys.* **96**, 893 (1999).

<sup>16</sup>A. Mori, S.-i. Yanagiya, Y. Suzuki, T. Sawada, and K. Ito, *J. Chem. Phys.* **124**, 174507 (2006).

<sup>17</sup>H. Chen and H. Ma, *J. Chem. Phys.* **125**, 024510 (2006).

<sup>18</sup>S. C. Kim and S. H. Suh, *J. Phys. Condens. Matter* **15**, 6617 (2003).

<sup>19</sup>J. P. Hoogenboom, P. Vergeer, and A. van Blaaderen, *J. Chem. Phys.* **119**, 3371 (2003).

<sup>20</sup>J. Hilhorst, J. R. Wolters, and A. V. Petukhov, *Cryst. Eng. Comm.* **12**, 3820 (2010).

<sup>21</sup>M. Marechal and M. Dijkstra, *Phys. Rev. E* **75**, 061404 (2007).

<sup>22</sup>J. W. Christian and V. Vitek, *Rep. Prog. Phys.* **33**, 307 (1970).

<sup>23</sup>S. Pronk and D. Frenkel, *J. Chem. Phys.* **110**, 4589 (1999).

<sup>24</sup>P. Heino, L. Perondi, K. Kaski, and E. Ristolainen, *Phys. Rev. B* **60**, 14625 (1999).

<sup>25</sup>J. Spitznagel and R. Stickler, *Metall. Mater. Trans. B* **5**, 1363 (1974).

<sup>26</sup>J. V. Sanders, *Acta Crystallogr.* **24**, 427 (1968).

<sup>27</sup>P. N. Pusey, W. van Megen, P. Bartlett, B. J. Ackerson, J. G. Rarity, and S. M. Underwood, *Phys. Rev. Lett.* **63**, 2753 (1989).

<sup>28</sup>J. P. Hoogenboom, D. Derks, P. Vergeer, and A. van Blaaderen, *J. Chem. Phys.* **117**, 11320 (2002).

<sup>29</sup>H. Miguez, F. Meseguer, C. López, A. Mifsud, J. S. Moya, and L. Vázquez, *Langmuir* **13**, 6009 (1997).

<sup>30</sup>Y. A. Vlasov, V. N. Astratov, A. V. Baryshev, A. A. Kaplyanskii, O. Z. Karimov, and M. F. Limonov, *Phys. Rev. E* **61**, 5784 (2000).

<sup>31</sup>W. K. Kegel and J. K.G. Dhont, *J. Chem. Phys.* **112**, 3431 (2000).

<sup>32</sup>V. C. Martelozzo, A. B. Schofield, W. C.K. Poon, and P. N. Pusey, *Phys. Rev. E* **66**, 021408 (2002).

<sup>33</sup>I. P. Dolbnya, A. V. Petukhov, D. G. A. L. Aarts, G. J. Vroege, and H. N. W. Lekkerkerker, *Europhys. Lett.* **72**, 962 (2005).

<sup>34</sup>L. Meng, H. Wei, A. Nagel, B. J. Wiley, L. E. Scriven, and D. J. Norris, *Nano Lett.* **6**, 2249 (2006).

<sup>35</sup>H. Wei, L. Meng, Y. Jun, and D. J. Norris, *Appl. Phys. Lett.* **89**, 241913 (2006).

<sup>36</sup>J. Zhu, M. Li, R. Rogers, W. Meyer, R. H. Ottewill, STS-73 Space Shuttle Crew, W. B. Russel, and P. M. Chaikin, *Nature (London)* **387**, 883 (1997).

<sup>37</sup>Z. Cheng, P. M. Chaikin, J. Zhu, W. B. Russel, and W. V. Meyer, *Phys. Rev. Lett.* **88**, 015501 (2001).

<sup>38</sup>Z. Cheng, J. Zhu, W. B. Russel, W. V. Meyer, and P. M. Chaikin, *Appl. Opt.* **40**, 4146 (2001).

<sup>39</sup>T. Okubo, A. Tsuchida, T. Okuda, K. Fujitsuna, M. Ishikawa, T. Morita, and T. Tada, *Colloids Surf. A* **153**, 515 (1999).

<sup>40</sup>M. Holgado, F. García-Santamaría, A. Blanco, M. Ibisate, A. Cintas, H. Míguez, C. J. Serna, C. Molpeceres, J. Requena, A. Mifsud, F. Meseguer, and C. López, *Langmuir* **15**, 4701 (1999).

<sup>41</sup>L. Filion, M. Hermes, R. Ni, and M. Dijkstra, *J. Chem. Phys.* **133**, 244115 (2010).

<sup>42</sup>C. Dux and H. Versmold, *Phys. Rev. Lett.* **78**, 1811 (1997).

<sup>43</sup>S. E. Paulin and B. J. Ackerson, *Phys. Rev. Lett.* **64**, 2663 (1990).

<sup>44</sup>B. W. van de Waal, *Phys. Rev. Lett.* **67**, 3263 (1991).

<sup>45</sup>P. Schall, I. Cohen, D. A. Weitz, and F. Spaepen, *Science* **305**, 1944 (2004).

<sup>46</sup>T. G. Andersson, Z. G. Chen, V. D. Kulakovskii, A. Uddin, and J. T. Vallin, *Appl. Phys. Lett.* **51**, 752 (1987).

<sup>47</sup>J. H. van der Merwe, *Crit. Rev. Solid State Mater. Sci.* **17**, 187 (1991).

<sup>48</sup>S. C. Mau and D. A. Huse, *Phys. Rev. E* **59**, 4396 (1999).

<sup>49</sup>M. Marechal and M. Dijkstra, *Soft Matter* **7**, 1397 (2011).

<sup>50</sup>A. van Blaaderen, J. Peetermans, G. Maret, and J. K. G. Dhont, *J. Chem. Phys.* **96**, 4591 (1992).

<sup>51</sup>W. van Megen and P. N. Pusey, *Phys. Rev. A* **43**, 5429 (1991).

<sup>52</sup>A. Fortini, E. Sanz, and M. Dijkstra, *Phys. Rev. E* **78**, 041402 (2008).

<sup>53</sup>V. W. A. de Villeneuve, Ph.D. thesis, Utrecht University, 2008.

<sup>54</sup>J.-M. Meijer, V. W. A. de Villeneuve, and A. V. Petukhov, *Langmuir* **23**, 3554 (2007).

- <sup>55</sup>V. W. A. de Villeneuve, P. S. Miedema, J. M. Meijer, and A. V. Petukhov, *EPL* **79**, 56001 (2007).
- <sup>56</sup>P. Strating, *Phys. Rev. E* **59**, 2175 (1999).
- <sup>57</sup>A. Scala, T. Voigtmann, and C. De Michele, *J. Chem. Phys.* **126**, 134109 (2007).
- <sup>58</sup>P. R. ten Wolde, M. J. Ruiz-Montero, and D. Frenkel, *Phys. Rev. Lett.* **75**, 2714 (1995).
- <sup>59</sup>W. Lechner and C. Dellago, *J. Chem. Phys.* **129**, 114707 (2008).
- <sup>60</sup>See the supplementary material at <http://dx.doi.org/10.1063/1.3609103> for a movie of the full evolution of the sediment.
- <sup>61</sup>M. Heni and H. Löwen, *Phys. Rev. E* **60**, 7057 (1999).